Smart Structures and Systems, *Vol. 17, No. 3 (2016) 413-429*
DOI: http://dx.doi.org/10.12989/sss.2016.17.3.413

Modal identifiability of a cable-stayed bridge using proper orthogonal decomposition

M. Li[a] and Y.Q. Ni[*]

Department of Civil and Environmental Engineering, The Hong Kong Polytechnic University, Hung Hom, Kowloon, Hong Kong

(Received June 22, 2015, Revised November 21, 2015, Accepted December 2, 2015)

Abstract. The recent research on proper orthogonal decomposition (POD) has revealed the linkage between proper orthogonal modes and linear normal modes. This paper presents an investigation into the modal identifiability of an instrumented cable-stayed bridge using an adapted POD technique with a band-pass filtering scheme. The band-pass POD method is applied to the datasets available for this benchmark study, aiming to identify the vibration modes of the bridge and find out the so-called deficient modes which are unidentifiable under normal excitation conditions. It turns out that the second mode of the bridge cannot be stably identified under weak wind conditions and is therefore regarded as a deficient mode. To judge if the deficient mode is due to its low contribution to the structural response under weak wind conditions, modal coordinates are derived for different modes by the band-pass POD technique and an energy participation factor is defined to evaluate the energy participation of each vibration mode under different wind excitation conditions. From the non-blind datasets, it is found that the vibration modes can be reliably identified only when the energy participation factor exceeds a certain threshold value. With the identified threshold value, modal identifiability in use of the blind datasets from the same structure is examined.

Keywords: cable-stayed bridge; modal identifiability; deficient mode; proper orthogonal decomposition; energy participation factor

1. Introduction

Vibration modal properties are common parameters widely used in structural dynamic response analysis, model updating, and vibration-based structural health evaluation. A variety of output-only modal analysis techniques have been proposed in the past decades. In recent years, proper orthogonal decomposition (POD) has gained attentions as a modal identification tool. The POD, also known as Karhunen–Loève decomposition, is a technique for extracting optimal distribution of energy from a set of multidimensional data (Jolliffe 2002). The earliest description of POD was first proposed by Pearson in 1901 (Pearson 1901) and then again by Hotelling in 1933 (Hotelling 1933). After its introduction, POD has steadily grown as a means to analyze complex physical systems. The widespread applications of POD methods make POD a popular tool in many fields

∗Corresponding author, Professor, E-mail: ceyqni@polyu.edu.hk
[a] Ph.D. Student, E-mail: ming.li.cse@connect.polyu.hk

http://www.techno-press.org/?journal=sss&subpage=8 ISSN: 1738-1584 (Print), 1738-1991 (Online)

(Fukagana 1972, Holmes 1990, Kunisch and Volkwein 1999).

In structural dynamics field, efforts have been made on physical interpretation of the proper orthogonal modes (POMs) and extracting structural vibration modes with POD methods. Feeny and Kappagantu (1998) proved that for discrete systems the POMs converge to linear normal modes (LNMs) in the case of undamped free vibration. Kerschen and Golinval (2002) came to a similar result by using singular value decomposition. Later on, the results have been extended to continuous vibration systems and randomly excited systems (Han and Feeny 2002, Feeny and Liang 2003). These works provided POD being a promising alternative to the traditional modal analysis methods. Since the singular values are related to the participating energy, the proper orthogonal coordinates can be treated as indicators of modal activity (Feeny 2001). However, several requirements should be satisfied when applying POD to modal identification. First, the mass matrix of the structure should be a constant multiple of the identity matrix, or at least must be known, which is difficult for practical applications. To overcome the limitation which requires *a priori* knowledge of the system's mass matrix, the smooth orthogonal decomposition (SOD) was proposed and demonstrated on undamped free vibration systems (Chelidze and Zhou 2006). This concept was then extended to randomly excited systems by Farooq and Feeny (2008).

According to Han (2000), due to spatial resolution, when applying POD on time-domain response data of a structure, only one POM represents the normal mode of the structure which has maximum contribution to the response (may not be the first or second mode). If one filters out the measured signals to contain only one target mode, then the POM extracted from the filtered signals converges to that particular mode of structure, regardless of the mass matrix (Han and Feeny 2003). The so-called band-pass POD has been successfully applied on a floating structure (Mariani and Dessi 2012). However, no studies of this method has been conducted on real infrastructure to evaluate its generalized applicability.

An investigation of modal identifiability of the cable-stayed Ting Kau Bridge (TKB) has recently been conducted (Ni *et al.* 2015). According to this study, a few modes failed to be reliably identified using the data acquired under weak wind conditions. It was found that when the excitation level in terms of average wind speed exceeded a certain threshold (around 7.5 m/s in this case), the deficient modes could be consistently identified. Later, taking the TKB as a test bed, a benchmark problem was launched and announced to interested investigators worldwide for the study on the mechanism behind output-only modal identifiability.

This paper provides a band-pass POD method to the benchmark study, in order to evaluate the applicability of this method on real infrastructure and verify the modal identifiability for potential deficient vibration modes. The band-pass POD method is applied to the dataset available in the benchmark study, aiming to identify the vibration modes of the TKB and observe the identifiability of deficient modes under different excitation conditions. The filtering scheme is first conducted to separate a particular mode from the response signals; then the POD method is executed to obtain the corresponding POM which converges to that particular mode. An energy participation factor based on modal coordinates identified from the band-pass POD is derived and energy participation patterns under different excitation conditions are compared. Making use of the energy participation factor, the reliability of identified mode shapes is examined.

2. Proper orthogonal decomposition (POD) and proper orthogonal modes (POMs)

2.1 Theory

The POD method extracts bases to decompose ensemble signals. In structural dynamics point of view, it is similar to the modal expansion theorem. In the modal expansion approach, the dynamic response of a structure is expressed as a linear combination of normal modes of the structure as follows

$$x(t)=\sum_{k=1}^{n}\{\phi\}_k\, q_k(t)=[\Phi]\{q\} \tag{1}$$

For the ensemble matrix

$$\mathbf{X}=\left[\mathbf{x}(t_1)\cdots\mathbf{x}(t_N)\right]=\left[\{q\}_1\{\phi\}_1^T+\cdots+\{q\}_n\{\phi\}_n^T\right] \tag{2}$$

each column represents the time history of displacement response measured at one point of the structure, where *n* is the number of measurement positions on the structure, vectors $\{q\}_k$ are $N\times 1$ arrays of the function $q_k(t)$ at times $t=t_1,t_2,\ldots t_N$, vectors $\{\phi\}_k$ are the normal modes discretized with *n* points on the structure.

The correlation matrix **R** is defined as

$$\mathbf{R}=\frac{1}{N}\mathbf{X}^T\mathbf{X} \tag{3}$$

To check whether a modal vector is actually a POM, one can multiply the correlation matrix **R** with the modal vector $\{\phi\}_j$ to obtain

$$[R]\{\phi\}_j=\frac{1}{N}[X]^T[X]\{\phi\}_j=\frac{1}{N}\left[\{q\}_1\{\phi\}_1^T+\cdots+\{q\}_n\{\phi\}_n^T\right]^T\left[\{q\}_1\{\phi\}_1^T+\cdots+\{q\}_n\{\phi\}_n^T\right]\{\phi\}_j \tag{4}$$

For mass-normalized modal vectors, the orthogonality condition is defined as

$$\{\phi\}_i^T[M]\{\phi\}_j=\delta_{ij}=\begin{cases}0 & \text{for } i\neq j\\ 1 & \text{for } i=j\end{cases} \tag{5}$$

When the mass matrix **M** is a constant multiple of the identity matrix, the orthogonality condition can be written as

$$\{\phi\}_i^T\{\phi\}_j=\delta_{ij}=\begin{cases}0 & \text{for } i\neq j\\ 1 & \text{for } i=j\end{cases} \tag{6}$$

Then Eq. (4) can be simplified as

$$[R]\{\phi\}_j=\frac{1}{N}\left(\{\phi\}_1\{q\}_1^T\{q\}_j+\cdots+\{\phi\}_n\{q\}_n^T\{q\}_j\right) \tag{7}$$

As $N\to\infty$, all $\{\phi\}_i\{q\}_i^T\{q\}_j/N$ will become zero except for the term $\{\phi\}_j\{q\}_j^T\{q\}_j$

which is proportional to $\{\phi\}_j$. Therefore the modal vector converges to the eigenvector of **R**, and thus a POM. The equation finally becomes

$$[R]\{\phi\}_j = \lambda_j \{\phi\}_j \tag{8}$$

where the eigenvalue $\lambda_j = \frac{1}{N}\{q\}_j^T \{q\}_j$.

When the structure system is formulated with its mass matrix being not proportional to the identity matrix, a transformation $\hat{\mathbf{R}} = \mathbf{RM}$ should be defined, and $\{\phi\}_j$ is a proper mode by multiplying $\hat{\mathbf{R}}$ by $\{\phi\}_j$.

2.2 Band-pass POD

The basic principle of treating POM as normal modal vector has several limitations as mentioned in the previous section. An adapted method has been proposed by filtering out the measured signals to contain only one particular mode (Feeny and Han 2003). When the particular normal mode is the most activated and contributes most, it can be identified by POD, regardless of the mass matrix. When the particular normal mode is not the most activated one, a filtering scheme can be conducted so that only the target mode contributes to the filtered signal. Thus the first POM of the band-pass POD becomes the corresponding linear normal mode.

Considering the signals consisting of only one particular mode, the dynamic responses measured at different points can be expressed as

$$[X] = \begin{Bmatrix} A\sin\omega_i t_1 \\ A\sin\omega_i t_2 \\ \vdots \\ A\sin\omega_i t_N \end{Bmatrix} \{\phi\}_i^T \tag{9}$$

Therefore the correlation matrix **R** is given as

$$\mathbf{R} = \frac{1}{N}\mathbf{X}^T\mathbf{X} = \{\phi\}_i \left(\frac{1}{N}\sum_{k=1}^{N} A^2 \sin^2 \omega_i t_k \right) \{\phi\}_i^T \tag{10}$$

Since the term $\frac{1}{N}\sum_{k=1}^{N} A^2 \sin^2 \omega_i t_k$ is the mean square value of a harmonic signal, the correlation matrix can be simplified as

$$\mathbf{R} = \frac{1}{N}\mathbf{X}^T\mathbf{X} = \left(rms\{q\}_i\right)^2 \{\phi\}_i \{\phi\}_i^T \tag{11}$$

where *rms* represents root mean square.

Since the rank of $\{\phi\}_i \{\phi\}_i^T$ is only one, its eigenvector is $\{\phi\}_i$ itself. In this case the normal

mode of the structure coincides with the POM extracted.

2.3 Energy participation factor

Once the *i*th normal mode $\{\phi\}_i$ is identified from the band-pass POD method, the modal coordinates $q_i(t)$ at times $t = t_1, t_2, \ldots t_N$ can be calculated from the equation

$$[X] = \{q\}_i \{\phi\}_i^T \tag{12}$$

With the modal coordinates, generalized energy in the *i*th mode is proportional to q_i^2. Define the average energy participated of the *i*th mode

$$E_i = \frac{1}{N} \sum_{k=1}^{N} q_i^2(t_k) \tag{13}$$

where $q_i(t_k)$ is the value of q_i at time t_k. After the energy for all concerned modes is calculated, the energy participation factor for the particular *i*th mode can be expressed as

$$f_{ep} = \frac{E_i}{\sum E_i} \tag{14}$$

With Eq. (14), the energy participation of each mode can be evaluated. As the energy participation changes with different excitations, the energy participation pattern can be recognized through comparing the results obtained from the different datasets. The energy participation factor can be used to determine the modal identifiability.

3. Ting Kau Bridge

3.1 TKB and SHM systems

The Ting Kau Bridge (TKB) in Hong Kong is a three-tower cable-stayed bridge with two main spans of 448 m and 475 m respectively, and two side spans of 127 m each (Bergermann and Schlaich 1996). The bridge deck has been separated into two carriageways with width of 18.8 m each. The two carriageways, with a 5.2 m gap, are linked at 13.5 m intervals by I-shape main crossgirders. Each carriageway grillage consists of two longitudinal steel girders along the deck edges with steel crossgirders at 4.5 m intervals, and a precast concrete deck panel on top. The three towers are 170 m, 194 m and 158 m respectively and composed of concrete structure with steel boxes attached to the top section. The deck is supported by 384 stay cables in four cable planes anchored to the deck edge girders at 13.5 m intervals. Eight longitudinal stabilizing cables, up to 464.6 m long, are used to diagonally connect the top of the central tower to the deck adjacent to the side towers. Because of the slenderness of the single-leg towers, both the central and side towers are also stiffened by a total of 64 transverse stabilizing cables in the lateral direction. Fig. 1 is a photo of TKB.

Fig. 1 Ting Kau Bridge

A sophisticated long-term monitoring system, called Wind And Structural Health Monitoring System (WASHMS), has been devised by the Highways Department of the Hong Kong SAR Government to monitor the structural health and performance of the bridge under in-service conditions (Wong 2004, Ko and Ni 2005). The WASHMS is composed of six integrated modules: sensory system, data acquisition and transmission system, data processing and control system, structural health evaluation system, structural health data management system, and inspection and maintenance system (Wong and Ni 2009). There are 24 uni-axial accelerometers, 20 bi-axial accelerometers, 1 tri-axial accelerometer, 7 anemometers (ultrasonic-type and propeller-type anemometers), 2 displacement transducers, 83 temperature sensors, 88 strain gauges (66 linear strain gauges and 22 rosette strain gauges) and a weigh-in-motion sensing system (with 6 sensors) permanently deployed on the bridge (Wong 2007, Ni *et al.* 2011).

The accelerometers were installed at the deck of two main spans, the Ting Kau side span deck, the Tsing Yi side span deck, the longitudinal stabilizing cables on the two main spans, the top of the three towers, and the base of central tower to measure the dynamic characteristics of the bridge. The layout of the accelerometers along the bridge deck and the sectional view are shown in Figs. 2 and 3. Fig. 4 shows a plan view of accelerometer placement on the bridge deck. Accelerometers No. 2, 5, 8, 11, 14, 17, 20, and 23 installed at central crossgirder measure the transverse acceleration, and the others measure the vertical acceleration. The sampling frequency was set as 25.6 Hz.

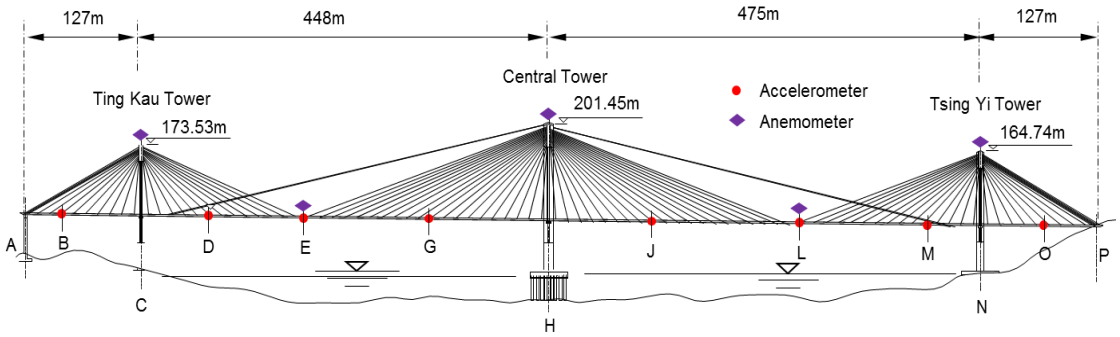

Fig. 2 TKB and layout of accelerometers on bridge deck

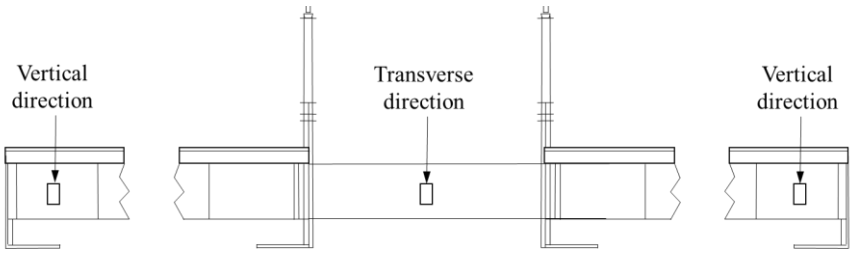

Fig. 3 Deployment of accelerometers on deck section

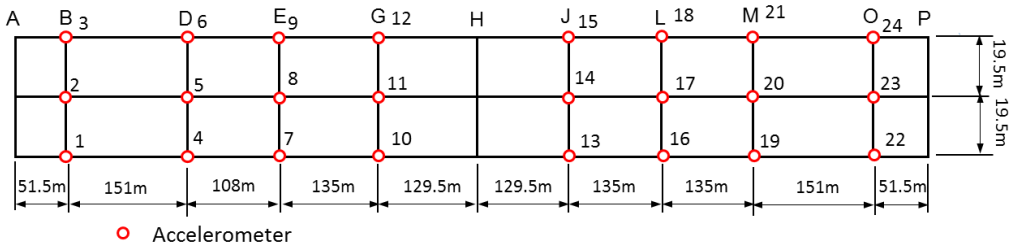

Fig. 4 Plan view of accelerometer placement on bridge deck

The anemometers were installed at the deck level of the two main spans and the top of the three towers to measure the wind speed and direction. There are four anemometers installed on the bridge deck and three anemometers at the top of the towers with a sampling frequency of 2.56 Hz.

3.2 Benchmark dataset

Ten sets of non-blind monitoring data, including both acceleration and wind speed/direction collected in different periods and under diverse excitation conditions are provided in this benchmark study, with 6 under weak wind excitations and 4 under typhoon excitations. In addition, three datasets under wind speed around the threshold value (7.5 m/s) are provided together with given wind speed conditions. The non-blind monitoring data provided are summarized in Table 1.

Six sets of blind data (acceleration responses only) without wind information are provided for evaluating the modal identifiability.

4. Results

4.1 Band-pass filtered signals

Fast Fourier transform (FFT) is conducted first to determine the frequencies of possible vibration modes, then band-pass filtering is carried out to extract acceleration data only containing the desired mode. The frequency for the first mode is around 0.162-0.166 Hz. As the frequency of the first mode is well separated from other modes, a width of 0.1-0.2 Hz is chosen for the band-pass filter. The original signal and the filtered signal at sensor nodes 7 and 11 from Sample 1

are plotted in Fig. 5. The POD is then conducted with the filtered signals and the POM is treated as the potential normal vibration mode.

Table 1 Thirteen non-blind data sets collected under different wind conditions

Condition	Sample	Time duration	Mean hourly wind speed (m/s)
Weak wind	Sample 1	15:00-16:00, 28 Dec 1999	2.00
	Sample 2	15:00-16:00, 18 Feb 1999	3.40
	Sample 3	15:00-16:00, 01 Mar 1999	3.34
	Sample 4	15:00-16:00, 21 Jun 1999	3.41
	Sample 5	15:00-16:00, 24 Jul 1999	6.17
	Sample 6	15:00-16:00, 12 Aug 1999	4.20
Typhoon	Maggie	03:00-04:00, 07 Jun 1999	12.11
	Sam	02:00-03:00, 23 Aug 1999	15.62
	York	06:00-07:00, 16 Sep 1999	21.72
	York	15:00-16:00, 16 Sep 1999	15.91
Around threshold	Jun07	08:00-09:00, 07 Jun 1999	7.36
	Sep16	22:00-23:00, 16 Sep 1999	7.77
	Sep26	09:00-10:00, 26 Sep 1999	7.43

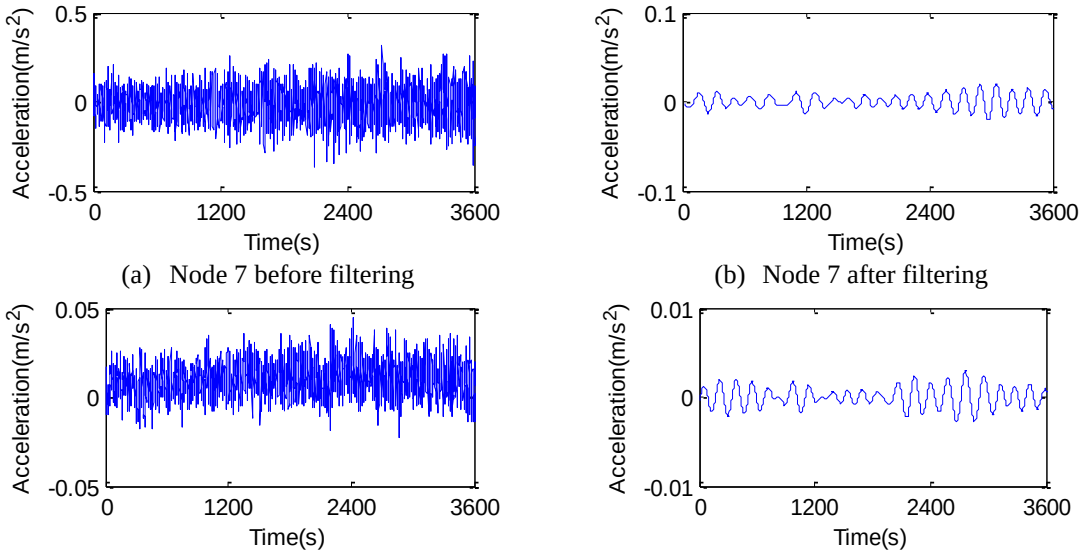

(a) Node 7 before filtering

(b) Node 7 after filtering

(c) Node 11 before filtering

(d) Node 11 after filtering

Fig. 5 Original signal and filtered signal at sensor nodes 7 and 11 from Sample 1

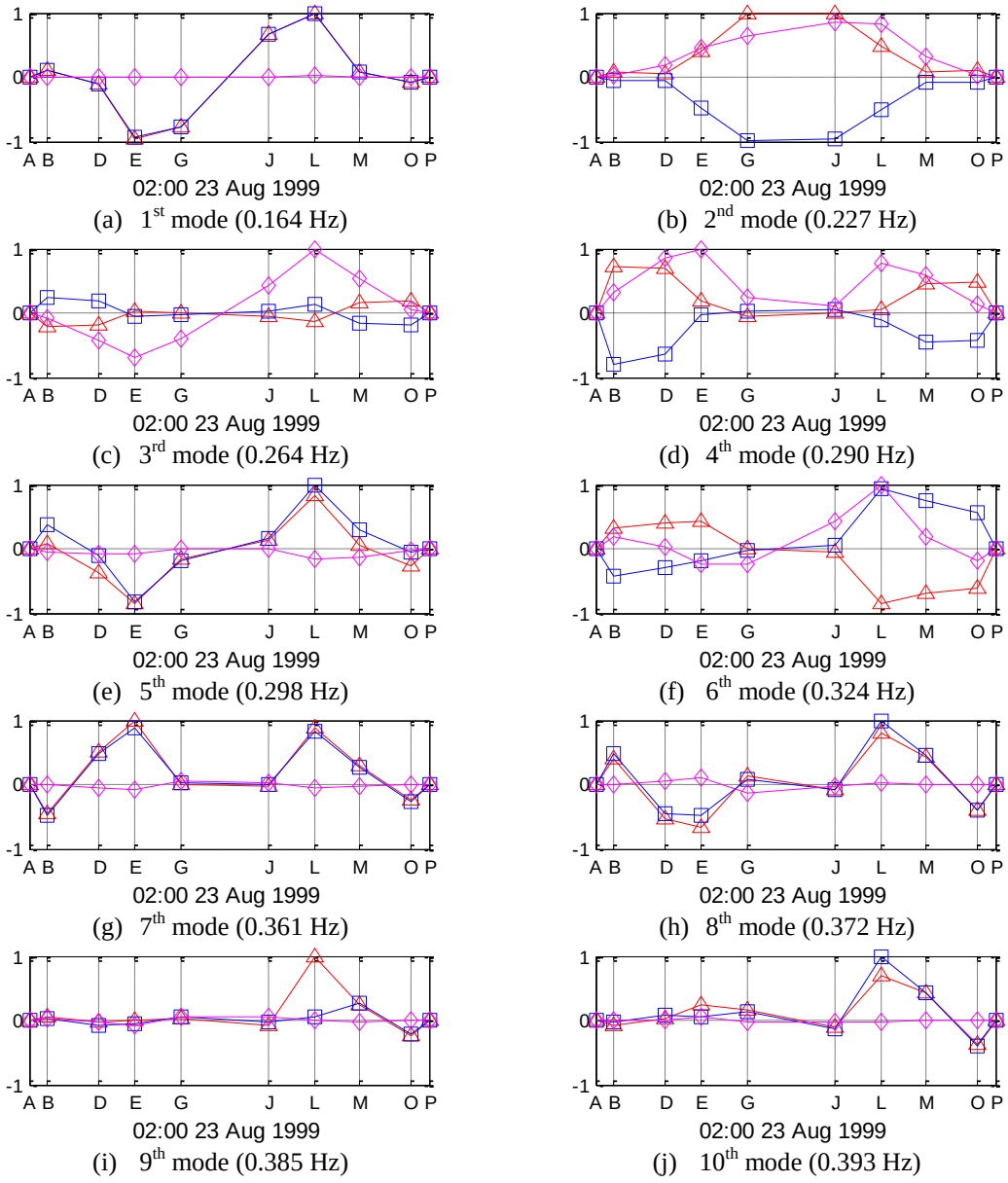

Fig. 6 Mode shapes of the first ten modes obtained under typhoon conditions

The first ten modes of vibration are extracted by the proposed method with the use of monitoring data acquired under typhoon conditions, as plotted in Fig. 6, where the vertical modal responses are plotted by lines with square and triangle symbols, while the transverse modal responses are plotted by lines with diamond symbols. The identified mode shapes by the present method coincide well with the results obtained in Ni *et al.* (2015), verifying the capability of the band-pass POD method in identifying mode shapes of real infrastructure.

4.2 Mode shapes of deficient modes

Modal identifiability of the second mode under both weak wind conditions and wind speed around 7.5 m/s are investigated using the band-pass POD method, with the results shown in Figs. 7 and 8.

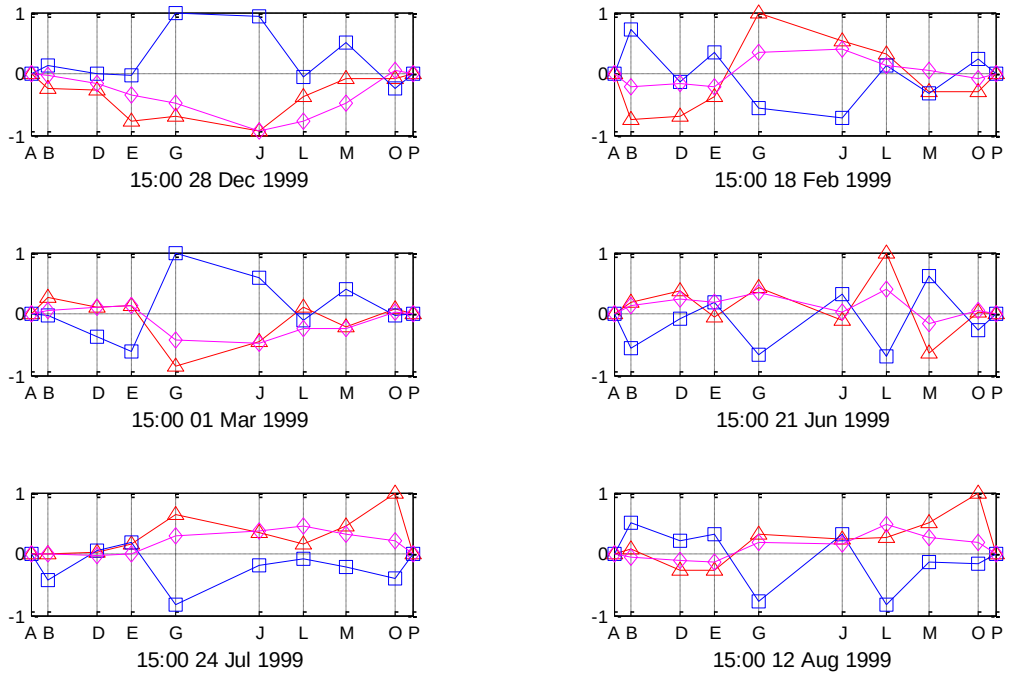

Fig. 7 Mode shapes of the second mode under weak wind conditions

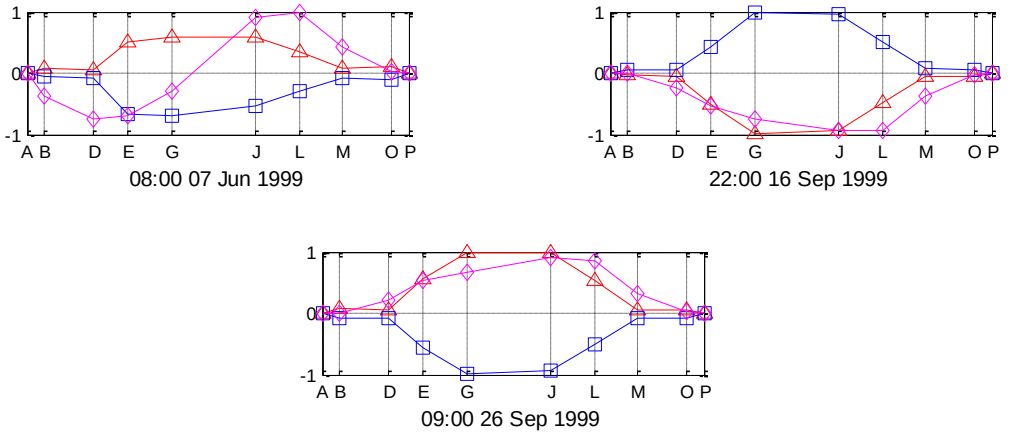

Fig. 8 Mode shapes of the second mode under wind speed around 7.5 m/s

The mode shape cannot be identified consistently under weak wind. In other words, this method fails to identify the mode shape of the second mode under weak wind conditions. The second mode is therefore a potential deficient mode.

Among the three datasets under wind speed around 7.5 m/s, the second mode can be identified successfully using the measured data from two datasets. However, the unidentifiable set still shows a pattern as semi-activated. From the results, it is reasonable to set 7.5 m/s wind speed as a threshold which makes the second mode identifiable.

4.3 Energy participation factor

With the obtained modal coordinates by the band-pass POD method as given in Eq. (12), the average energy and participation factor for each mode can be calculated using Eqs. (13) and (14) for the cases under different wind conditions. The results are listed in Table 2. Energy distributions under both typhoon and weak wind conditions are plotted in Fig. 9.

According to Table 2 and Fig. 9, it is clear that the datasets under same wind conditions share similar energy distribution patterns. The fundamental mode participates most among the first ten modes in despite of wind condition, while the energy participation factor of second mode changes significantly under both typhoon and weak wind conditions. Under typhoon conditions, the second mode has a larger energy participation factor (larger than 3.0% as given in Table 2), which is consistent with the fact that it is identifiable. While under weak wind conditions, the energy participation factor of second mode is only about 0.1% to 0.2%, suggesting that the second mode is almost not activated, which explains the phenomenon that the second mode cannot be identified consistently under weak wind conditions. Meanwhile, the energy participation factor obtained when the wind speed is around 7.5 m/s falls between weak wind cases and typhoon cases.

Table 2 Energy participation factor for different modes under different wind conditions

	Mode No.	1	2	3	4	5	6	7	8	9	10
Typhoon	**Maggie**	66.2%	4.0%	3.4%	3.4%	1.0%	5.1%	9.9%	5.0%	0.8%	1.0%
	Sam	41.0%	3.5%	3.2%	1.9%	1.3%	4.1%	27.8%	13.8%	1.1%	2.3%
	York1	44.2%	3.0%	0.9%	1.8%	2.0%	3.4%	32.7%	8.0%	1.8%	2.2%
	York2	28.8%	10.7%	6.3%	7.4%	0.8%	16.8%	22.1%	5.6%	0.9%	0.6%
Weak wind	**S1**	69.0%	0.2%	1.3%	1.7%	0.6%	0.1%	19.1%	7.2%	0.4%	0.4%
	S2	73.0%	0.2%	0.9%	1.7%	0.7%	0.4%	15.8%	6.2%	0.6%	0.4%
	S3	65.3%	0.2%	2.0%	1.5%	0.6%	0.3%	19.6%	9.1%	0.7%	0.7%
	S4	67.4%	0.1%	2.3%	1.8%	0.7%	1.0%	17.7%	8.1%	0.5%	0.4%
	S5	54.8%	0.2%	1.3%	1.5%	0.8%	0.8%	30.8%	8.9%	0.4%	0.7%
	S6	57.0%	0.2%	2.6%	0.7%	0.6%	1.5%	27.6%	8.4%	0.6%	0.7%
Around 7.5 m/s	**7-Jun**	49.6%	0.9%	0.1%	0.3%	1.1%	1.0%	37.3%	8.1%	0.7%	1.1%
	16-Sep	52.2%	2.8%	7.1%	4.4%	1.6%	11.9%	14.6%	3.6%	0.7%	1.3%
	26-Sep	32.1%	10.5%	10.3%	18.8%	0.7%	16.6%	8.1%	2.1%	0.4%	0.6%

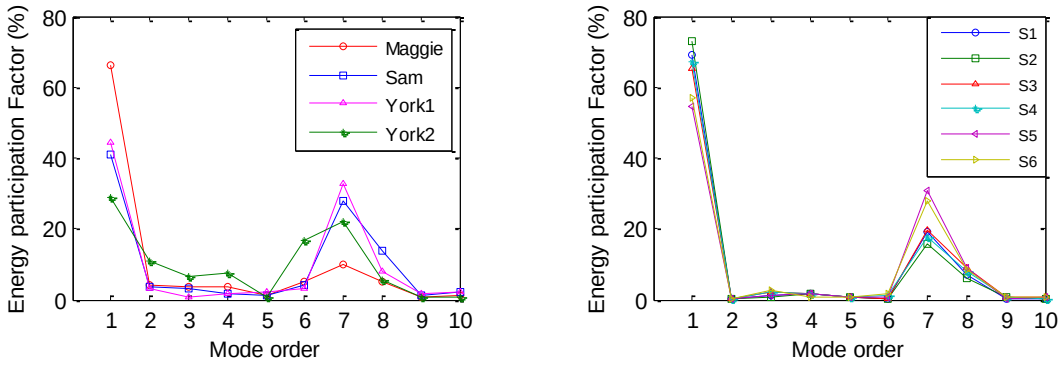

(a) Typhoon conditions (b) Weak wind conditions

Fig. 9 Energy distribution under different wind conditions

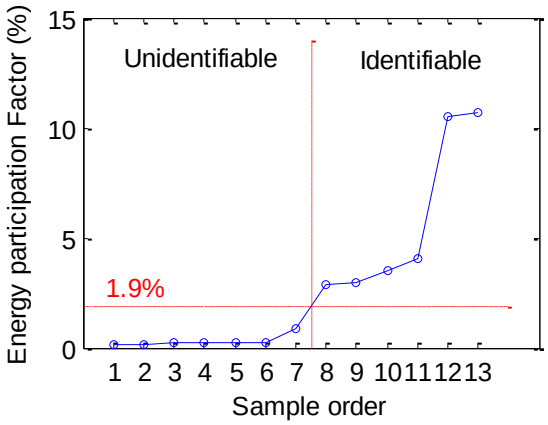

Fig. 10 Threshold of energy participation factor

The energy participation factor of the second mode for all the thirteen non-blind datasets are plotted in Fig. 10. Based on these results, a threshold value for energy participation factor is determined as about 1.9%. When the energy participation factor is larger than 1.9%, the identified second mode is reliable. Contrarily, when the energy participation factor is lower than 1.9%, the identified second mode is unreliable with inconsistent mode shape. In a word, the energy participation factor can be used as an indicator to examine the modal identifiability of the second mode.

The energy participation factor as an indicator of modal identifiability also works for other modes. Since the second mode can be consistently identified only under certain conditions, the energy participation factor changes significantly depending on different wind conditions (Fig. 11(a)). While for other modes, which can be identified consistently under both weak wind and

typhoon conditions, there is no significant variation in energy participation factor among different datasets (Fig. 11(b)). The difference can be found clearly from Fig. 11. It should be noted that the threshold value of 1.9% is just an indicator to evaluate the reliability of the second mode. As for other modes, the threshold value can be higher or lower than 1.9%. For example, as evidenced in Fig. 11(b), the fifth mode is identifiable when its energy participation factor is higher than 0.5% (the threshold value for the fifth mode might be even less than this value).

4.4 Blind datasets

In the benchmark study, six sets of blind data are provided for participants to verify the modal identifiability without knowledge of wind conditions. By applying the band-pass POD method, the mode shape vectors of the second mode are obtained from the six blind datasets as plotted in Fig. 12. The obtained values of the energy participation factor for different modes are given in Table 3 to verify the modal identifiability.

Table 3 Energy participation factor for different modes obtained from blind data

	Mode No.	**1**	**2**	**3**	**4**	**5**	**6**	**7**	**8**	**9**	**10**
	Acc1	47.0%	11.3%	4.9%	9.8%	1.9%	8.6%	12.0%	2.5%	0.8%	1.3%
	Acc2	43.3%	6.4%	5.8%	5.3%	1.4%	11.6%	13.8%	9.0%	1.7%	1.5%
Blind	**Acc3**	58.6%	0.7%	0.2%	0.5%	1.4%	1.0%	30.7%	5.8%	0.4%	0.7%
data	**Acc4**	54.5%	2.2%	6.2%	3.2%	1.0%	9.4%	16.3%	4.9%	1.2%	1.1%
	Acc5	63.9%	0.1%	2.3%	1.9%	0.5%	0.3%	23.2%	6.8%	0.8%	0.3%
	Acc6	57.7%	0.3%	1.3%	0.9%	0.6%	0.8%	30.9%	6.7%	0.4%	0.5%

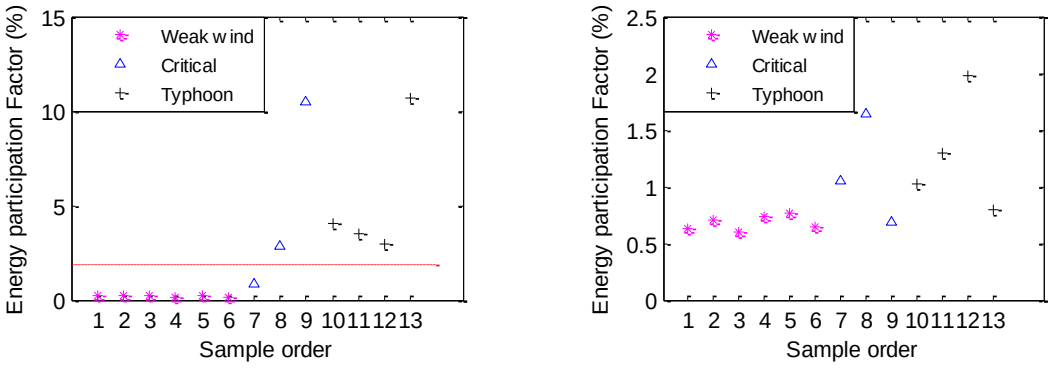

(a) Second mode (b) Fifth mode

Fig. 11 Energy participation factor of the second and fifth modes

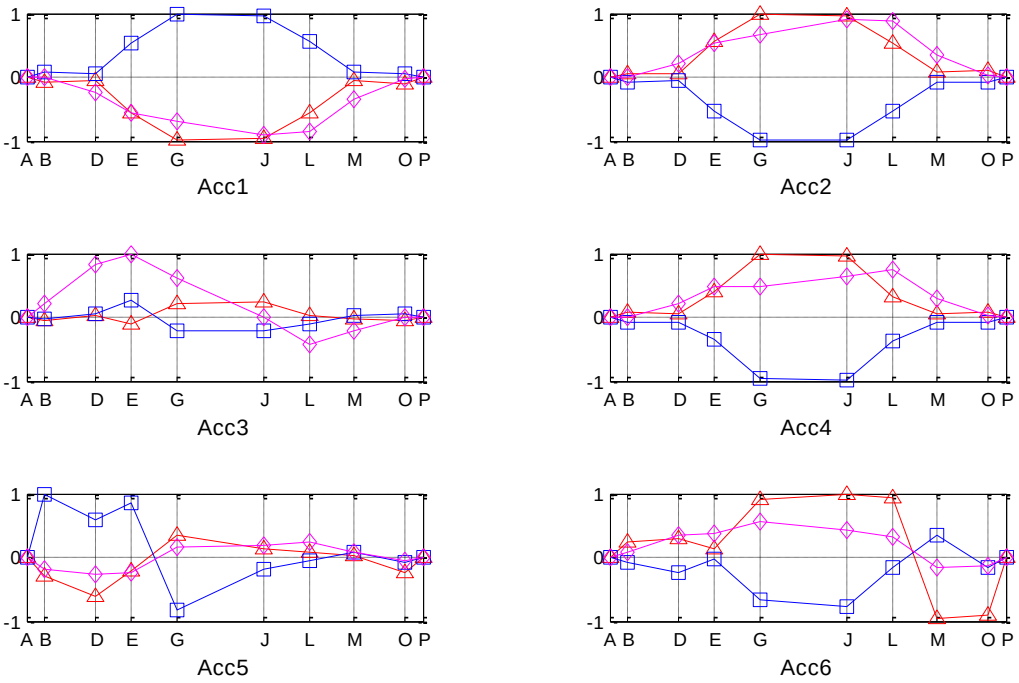

Fig. 12 Mode shapes of the second mode obtained from blind data

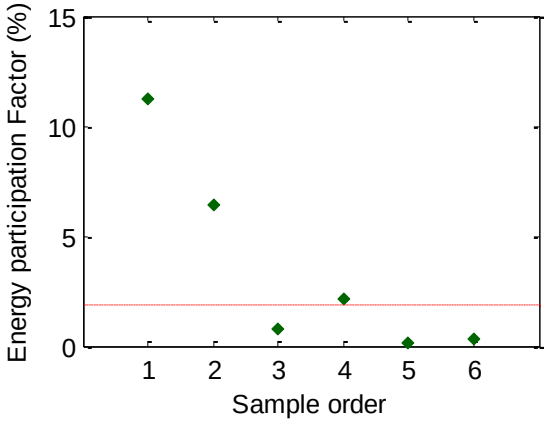

Fig. 13 Energy participation factor of the second mode

Fig. 13 plots the energy participation factor of the second mode obtained from the blind data, in conjunction with the threshold line (at the ordinate of 1.9%) previously determined by the non-blind data. From this figure, it is deduced that the second mode shape identified using the datasets Acc1

and Acc2 should be highly reliable because the energy participation factor resulting from these two datasets is much larger than the threshold value; the mode shape identified using the dataset Acc4 might be marginal because the energy participation factor is close to the threshold; and the datasets Acc3, Acc5 and Acc6 would give rise to unreliable modal identification result because of their low energy participation factor. By comparing Fig. 12 with Fig. 6, it is observed that the mode shapes identified using the datasets Acc1, Acc2 and Acc4 indeed agree well with the mode shape identified using the non-blind data under typhoon conditions. Moreover, the identified mode shapes using the datasets Acc3, Acc5 and Acc6, which are inconsistent with each other and distinct from that identified using the non-blind data under typhoon conditions, truly reflect their incapability in identifying the mode shape with fidelity. The above observations justify that the energy participation factor derived from the band-pass POD is workable to evaluate the modal identifiability, especially for distinguishing between the anomaly in identified mode shapes due to deficient modes and the change in mode shapes caused by structural damage and excluding the abnormally identified modes when dealing with long-term monitoring data.

5. Conclusions

Presented in this paper was a study on the modal identifiability of a cable-stayed bridge using an adapted POD technique with a band-pass filtering scheme. The long-term monitoring data acquired from the cable-stayed Ting Kau Bridge (TKB), where deficiency in output-only modal identification has been observed in the previous study, were used for a benchmark study. The band-pass POD method adopted in this study also confirmed the incapability in reliably identifying certain vibration modes (mode vectors) using the dynamic response data acquired under normal ambient excitations. In this connection, an energy participation factor was derived from the band-pass POD to characterize the energy level of individual modes and explore its relevance to the modal identifiability with the use of non-blind monitoring data (both acceleration and wind speed) obtained under different wind conditions. It has been shown that there is a threshold value of the energy participation factor for each deficient mode, above which the mode shape can be reliably identified from ambient vibration response.

Six blind datasets of acceleration responses acquired from the same structure, without knowledge of wind conditions, have been used to verify the feasibility of using the energy participation factor and its threshold to judge the modal identifiability. The derived values of the energy participation factor deduce that two blind datasets are able to reliably identify the mode shape for the deficient mode, one blind dataset is marginal in identifying the deficient mode, and three blind datasets would give rise to unreliable mode shape identification for the deficient mode. The above deduction has been agreeably validated through a comparison between the mode shapes identified from the blind datasets and those obtained from the non-blind datasets under typhoon conditions. On the basis of a statistical comparison between the energy participation factor values for different modes obtained from non-blind datasets and those from a blind dataset, it is also possible to classify the level of excitation which generates the blind dataset. The study presented in this paper is helpful to distinguish between the anomaly in identified mode shapes due to deficient modes and the change in mode shapes caused by structural damage and get rid of the abnormally identified modes in dealing with long-term structural health monitoring data to avoid false-positive damage detection.

Acknowledgments

The work described in this paper was supported by a grant from the Research Grants Council of the Hong Kong Special Administrative Region, China (Project No. PolyU 5224/13E). The writers also wish to thank the Hong Kong SAR Government Highways Department for providing the long-term structural health monitoring data of the Ting Kau Bridge.

References

Bergermann, R. and Schlaich, M. (1996), "Ting Kau Bridge, Hong Kong", *Struct. Eng. Int.*, **6**(3), 152-154.
Chelidze, D. and Zhou, W. (2006), "Smooth orthogonal decomposition-based vibration mode identification", *J. Sound Vib.*, **292**(3), 461-473.
Farooq, U. and Feeny, B.F. (2008), "Smooth orthogonal decomposition for modal analysis of randomly excited systems", *J. Sound Vib.*, **316**(1), 137-146.
Feeny, B.F. (2002), "On proper orthogonal co-ordinates as indicators of modal activity", *J. Sound Vib.*, **255**(5), 805-817.
Feeny, B.F. and Kappagantu, R. (1998), "On the physical interpretation of proper orthogonal modes in vibrations", *J. Sound Vib.*, **211**(4), 607-616.
Feeny, B.F. and Liang, Y. (2003), "Interpreting proper orthogonal modes of randomly excited vibration systems", *J. Sound Vib.*, **265**(5), 953-966.
Fukagana, K. (1972), *Introduction to Statistical Pattern Recognition*, Academic Press, New York.
Han, S. (2000), "Linking proper orthogonal modes and normal modes of the structure", *Proceedings of the IMAC 18*, San Antonio, TX.
Han, S. and Feeny, B.F. (2002), "Enhanced proper orthogonal decomposition for the modal analysis of homogeneous structures", *J. Sound Vib.*, **8**(1), 19-40.
Han, S. and Feeny, B. (2003), "Application of proper orthogonal decomposition to structural vibration analysis", *Mech. Syst. Signal Pr.*, **17**(5), 989-1001.
Holmes, J.D. (1990), "Analysis and synthesis of pressure fluctuations on bluff bodies using eigenvectors", *J. Wind. Eng. Ind. Aerod.*, **33**(1-2), 219-230.
Hotelling, H. (1933), "Analysis of a complex of statistical variables into principal components", *J. Educ. Psychol.*, **24**(6), 417-441.
Jolliffe, I.T. (2002), *Principal Component Analysis*, 2nd Ed., Springer, New York.
Kerschen, G. and Golinval, J.C. (2002), "Physical interpretation of the proper orthogonal modes using the singular value decomposition", *J. Sound Vib.*, **249**(5), 849-865.
Kunisch, K. and Volkwein, S., (1999), "Control of the Burgers' equation by a reduced order approach using proper orthogonal decomposition", *J. Optimiz. Theory App.*, **102**, 345-371.
Ko, J.M. and Ni, Y.Q. (2005), "Technology developments in structural health monitoring of large-scale bridges", *Eng. Struct.*, **27**(12), 1715-1725.
Mariani, R. and Dessi, D. (2012), "Analysis of the global bending modes of a floating structure using the proper orthogonal decomposition", *J. Fluid Struct.*, **28**, 115-134.
Ni, Y.Q., Wang, Y.W. and Xia, Y.X. (2015), "Investigation of mode identifiability of a cable-stayed bridge: comparison from ambient vibration responses and from typhoon-induced dynamic responses", *Smart Struct. Syst.*, **15**(2), 447-468.
Ni, Y.Q., Wong, K.Y. and Xia, Y. (2011), "Health checks through landmark bridges to sky-high structures", *Adv. Struct. Eng.*, **14**(1), 103-119.
Pearson, K. (1901), "On lines and planes of closest fit to systems of points in space", *Phil. Mag.*, **2**, 559-572.
Wong, K.Y. (2004), "Instrumentation and health monitoring of cable-supported bridges", *Struct. Control. Health Monit.*, **11**(2), 91-124.

Wong, K.Y. (2007), "Design of a structural health monitoring system for long-span bridges", *Struct. Infrastruct. E.*, **3**(2), 169-185.
Wong, K.Y. and Ni, Y.Q. (2009), "Modular architecture of structural health monitoring system for cable-supported bridges", *Encyclopedia of Structural Health Monitoring*, (Eds., C. Boller, F.K. Chang and Y. Fujino), John Wiley & Sons, Chichester, UK, **5**.